Cancer Nanotechnology

RESEARCH Open Access

Reprogramming tumor microenvironment via dual targeting co-delivery of regorafenib and alpha-difluoromethylornithine in osteosarcoma

Hongsheng Wang[1†], Xinmeng Jin[1†], Yinghua Gao[1†], Xin He[1], Yiming Xu[1], Haoran Mu[1], Yafei Jiang[1], Zhuoying Wang[1], Chen Yu[1,2], Tao Zhang[1], Yingqi Hua[1], Zhengdong Cai[1], Jing Xu[1*], Xiaojun Ma[1*] and Wei Sun[1*]

[†]Hongsheng Wang and Xinmeng Jin and Yinghua Gao contributed equally to this work

*Correspondence: jingxu6000@163.com; ma-xiaojun@foxmail.com; vivsun@sjtu.edu.cn

[1] Department of Orthopaedics, Shanghai Bone Tumor Institute, Shanghai General Hospital, Shanghai Jiao Tong University School of Medicine, Shanghai 200080, China
[2] Department of Orthopaedics, Sir Run Run Hospital, Nanjing Medical University, Nanjing 211100, China

Abstract

Background: Tumor angiogenesis, immunosuppression, and progression are all closely correlated with the tumor microenvironment (TME). Immune evasion is supported by both M2 phenotype tumor-associated macrophages (TAMs) and vascular aberrations in the TME. TME reprogramming is a promising therapeutic approach for treating tumors. Anti-angiogenesis has the power to control the polarization of macrophages, prevent progression, and increase drug penetration. Additionally, polyamine blocking therapy can increase $CD8^+$T cell infiltration and decrease immunosuppressive cells. These results led to developing a potential therapeutic regimen that targets TAMs and angiogenesis to reprogram the osteosarcoma TME.

Results: For the targeted biomimetic co-delivery of regorafenib and alpha-difluoromethylornithine via the mannose receptor, which is overexpressed in both TAMs and osteosarcoma cells, mannosylated poly(lactide-co-glycolide)-polyethylene glycol nanoparticles (Man-NPs) were synthesized. The superior physiological properties and intratumoral accumulation of the Man-NPs efficiently promoted TAMs polarization and inhibited angiogenesis. Macrophage repolarization further activated immune cells, which contributed to remodeling the TME.

Conclusion: Overall, these findings suggested that using Man-NPs as an immunotherapeutic approach to treat osteosarcoma may be promising.

Keywords: Drug co-delivery, Tumor microenvironment, Tumor-associated macrophages, Anti-angiogenesis, Osteosarcoma

Graphical Abstract

© The Author(s) 2023. **Open Access** This article is licensed under a Creative Commons Attribution 4.0 International License, which permits use, sharing, adaptation, distribution and reproduction in any medium or format, as long as you give appropriate credit to the original author(s) and the source, provide a link to the Creative Commons licence, and indicate if changes were made. The images or other third party material in this article are included in the article's Creative Commons licence, unless indicated otherwise in a credit line to the material. If material is not included in the article's Creative Commons licence and your intended use is not permitted by statutory regulation or exceeds the permitted use, you will need to obtain permission directly from the copyright holder. To view a copy of this licence, visit http://creativecommons.org/licenses/by/4.0/. The Creative Commons Public Domain Dedication waiver (http://creativecommons.org/publicdomain/zero/1.0/) applies to the data made available in this article, unless otherwise stated in a credit line to the data.

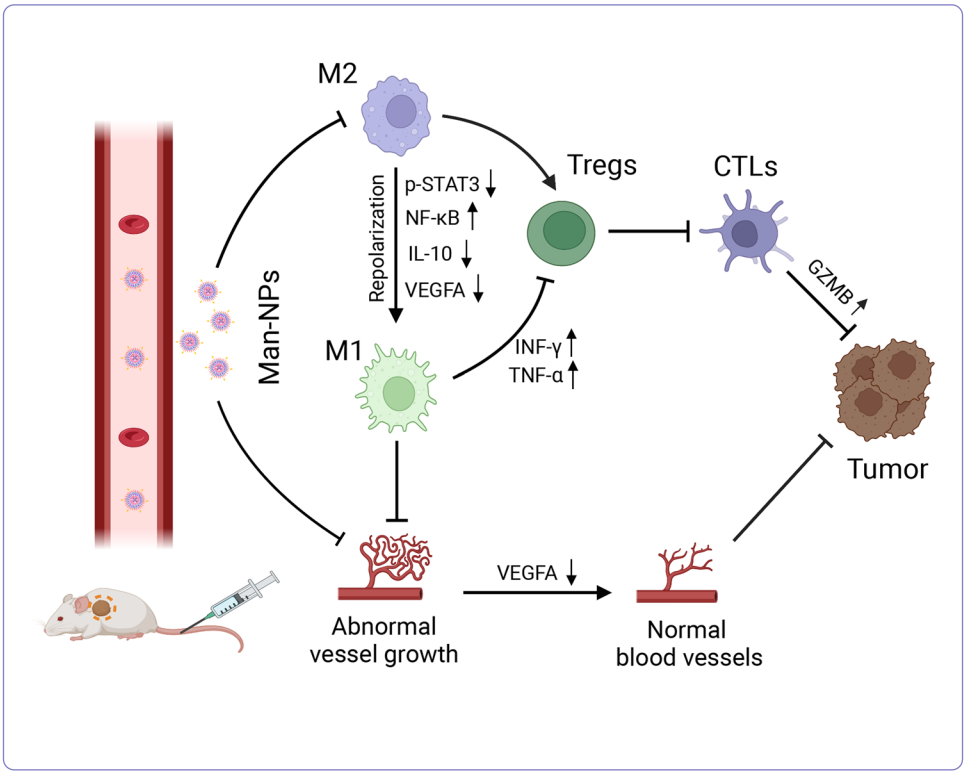

Background

The most common age groups for osteosarcoma (OS), a primary bone malignant tumor with mesenchymal tissue origin, are children and adolescents (Gill et al. 2021). The standard of care for patients with OS is surgery in combination with neo-adjuvant and adjuvant chemotherapeutic drugs, which appropriately provides 70% of patients a 5-year nonmetastatic survival rate. However, patients with lung metastasis had a five-year survival rate of less than 30% (Liu et al. 2021; Marchandet et al. 2021). Recently, immunotherapy has significantly changed how cancer is treated (Dallavalasa et al. 2021). The effectiveness of immunotherapy relies on tumor cells and the host immune system working together effectively. However, due to the low expression of PD-L1, osteosarcoma is regarded as a relatively "cold tumor", demonstrating a poor response to immune checkpoint inhibitors PD-1 and PD-L1 (Galon et al. 2019; Tawbi et al. 2017). It is therefore widely accepted that altering the tumor immune microenvironment (TIME) is a potential strategy for triggering the body's defenses against osteosarcoma.

As the majority of infiltrating immune cells in the tumor microenvironment (TME), tumor-associated macrophages (TAMs) have been used as a prognostic indicator and a new target for tumor immunotherapy (Koirala et al. 2016). M1 phenotype macrophages (termed TAM1) are thought to be anti-tumorigenic because they release cytotoxic chemicals and cytokines and promote T cell immunity (Cersosimo et al. 2020; Le et al. 2021). In contrast, M2 phenotype macrophages (termed TAM2) promote tumor angiogenesis and immune escape, ultimately leading to tumor progression and metastasis (Cersosimo et al. 2020; Le et al. 2021). However, tumor

angiogenesis can also regulate the immune response by polarizing macrophages with the M2 phenotype and suppressing the immune system (Okikawa et al. 2022).

Inhibition of neovascularization by blocking the VEGF/VEGFR signaling pathway using multi-kinase inhibitors and anti-vascular endothelial growth factor (VEGF) monoclonal antibodies is a therapeutic strategy that influences immune cell populations in the TME. Regorafenib, a multi-kinase inhibitor with Food and Drug administration (FDA) approval, inhibits tumor progression by targeting the activity of oncogenic kinases that control cell signal transduction and tumor angiogenesis (Duffaud et al. 2019). More importantly, regorafenib could convert TAMs from M2 to M1 phenotype, induce T cell activation, and combine with anti-PD-1 sensitized tumors to produce synergistic immunomodulatory effects (Chiang et al. 2022; Doleschel et al. 2021; Ou et al. 2021). However, molecules that interfere with VEGF/VEGFR signaling are responsible for severe adverse effects because of inhibition of physiological angiogenesis (Lacal et al. 2018). Regorafenib significantly increased progression-free survival in phase II trials in patients with advanced osteosarcoma compared to placebo, but there was no appreciable statistical difference in overall survival (Davis et al. 2019). Here, a shift from a single- to a multi-target therapeutic approach is essential to trigger the host immune system and provide long-term efficacy.

Anti-angiogenic therapy has been proven to have some effect on TME, and recent literature suggests that additional drug therapies may also be able to modulate the immune system. Particularly, tumor progression in immunocompetent tumor-bearing mice was significantly suppressed by polyamine blocking therapy (PBT), which involved the inhibition of polyamine biosynthesis and transport (Hayes et al. 2014). During cellular processes, alpha-difluoromethylornithine (DFMO) is an FDA-approved inhibitor that inhibits ornithine decarboxylase and blocks polyamine biosynthesis (Pfeffer et al. 2000). In immunocompetent mice, DFMO therapy has been shown to inhibit tumor growth by increasing $CD8^+$ T cell infiltration and reducing myeloid-derived suppressor cells activity (Ye et al. 2016). Furthermore, it has undergone favorable evaluation in clinical trials for the treatment and chemoprevention of neuroblastoma (Lewis et al. 2020; Samal et al. 2013; Sholler et al. 2018). Therefore, combining anti-angiogenic therapy with PBT may be a viable option to increase the effectiveness of immunotherapy, reduce the likelihood of drug side effects, and remodel the osteosarcoma TME.

In this study, we designed mannosylated poly(lactide-co-glycolide)-polyethylene glycol (PLGA-PEG) nanoparticles (Man-NPs) for biomimetic regorafenib and DFMO delivery that target the TME and remodel it. TAM2 and K7 osteosarcoma cells could specifically recognize and phagocytize the NPs due to the overexpression of CD206 on both types of cells. In vitro evaluations of Man-NPs' physicochemical properties, regulation of TAM2 repolarization, and angiogenesis were thorough. To assess the in vivo tissue distribution and anti-tumor effectiveness of Man-NPs, we established a xenograft osteosarcoma model given the high degree of osteosarcoma malignancy. We discovered that Man-NPs accumulated more effectively in tumors, promoting the polarization of TAMs, the infiltration of $CD8^+$ T cells, and the reduction of Tregs populations via anti-angiogenesis and PBT (Scheme 1) (created with BioRender.com).

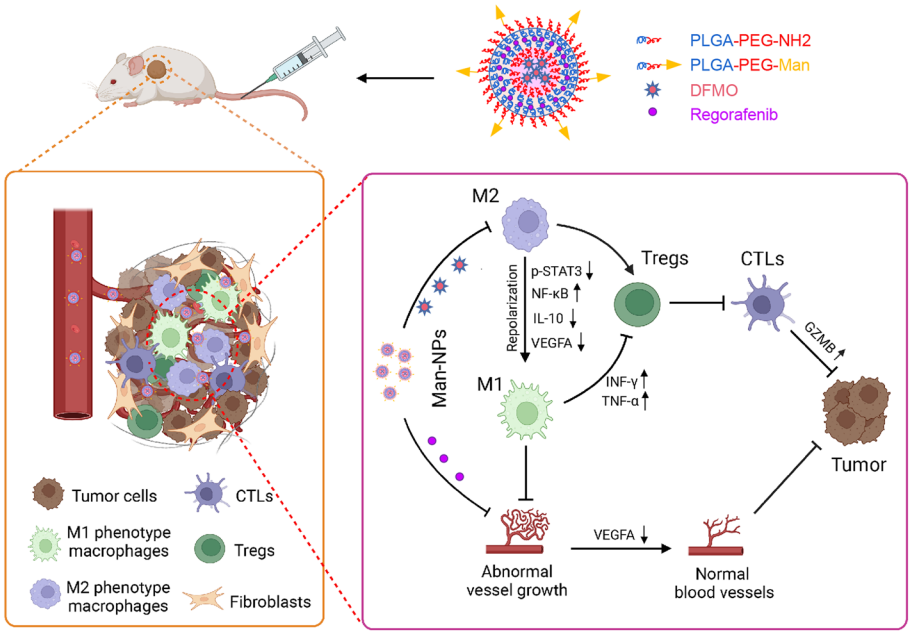

Scheme 1 Schematic representation of tumor immunotherapy using Man-NPs, which regulates tumor-associated macrophages and angiogenesis in tandem to target the tumor microenvironment

These findings offer a promising new strategy for TAMs-targeted immunotherapy and anti-angiogenesis that can effectively inhibit tumor growth by remodeling the TME.

Results and discussion

Properties and characterization of Man-NPs

The mannose receptor, also named as CD206, is one of the most frequently used TAMs-targeted receptors, owing to its high expression in TAM2. As shown in Fig. 1a, TAM2 and, importantly, K7 cells both expressed CD206 at high levels. As a result, mannose-modified NPs that target TAMs and osteosarcoma cells can be designed rationally because they have a physiological bias. In the current study, mannose was conjugated with PLGA-PEG as a targeted ligand of TAM2 and osteosarcoma cells based on the specific identification of mannose receptors. The H^1NMR spectrum was used to determine the man-PLGA-PEG co-polymer (Additional file 1: Fig. S1). A double emulsion solvent evaporation method successfully created the mannosylated nanoparticles enclosed in regorafenib/DFMO. Man-NPs had an average particle size of 146 nm, while unmodified PLGA-PEG nanoparticles, or NPs, had a particle size of 125 nm (Fig. 2b, c). The partial neutralization of the negative charge by mannose caused the zeta potentials of NPs to change after the mannose modification from − 23.3 mV to − 10.6 mV (Additional file 1: Fig. S2a). Man-NPs and NPs exhibited low PDI values (< 0.3), indicating narrow distribution of molecular weight (Additional file 1: Fig. S2b). The drug encapsulation efficiency of Man-NPs was 77.68% for DFMO and 74.6% for regorafenib, and the drug-loading efficiency was 2.9% and 0.6%, respectively. Man-NPs also displayed a sustained-release pattern (Fig. 1d). In 10% FBS, the Man-NPs displayed good stability (Additional file 1: Fig. S2c), which is appropriate for their biomedical applications.

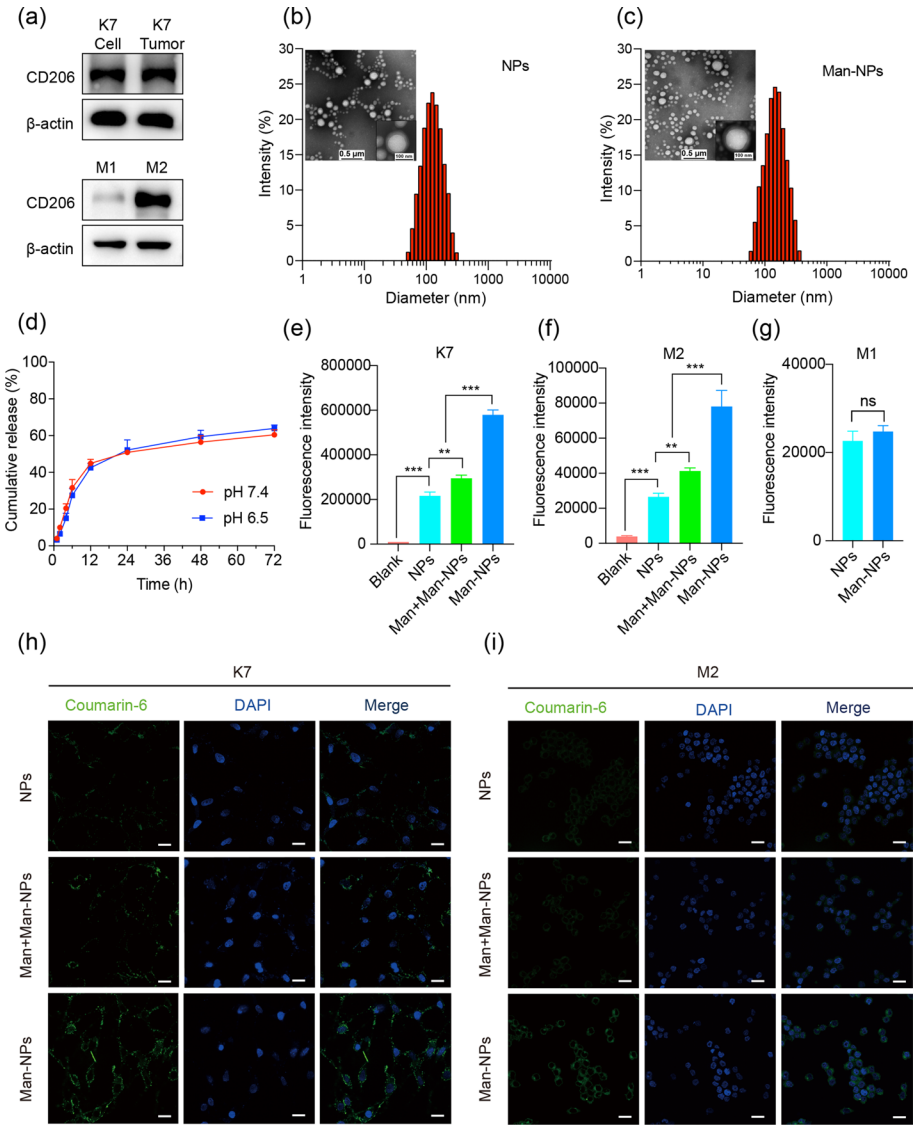

Fig. 1 In vitro characterization of Man-NPs. **a** CD206 expression in K7 cells, K7 tumor, M1 and M2 phenotype macrophages. Size distribution and TEM image of the NPs (**b**) and Man-NPs (**c**). **d** Cumulative release of regorafenib in Man-NPs. Uptake efficiency of NPs and Man-NPs with or without pretreatment with mannose in K7 cells (**e**), TAM2 (**f**), and TAM1 (**g**). Representative CLSM images of K7 cells (**h**) and M2 phenotype macrophage (**i**) after 6 h of incubation with the Coumarin-6-loaded NPs (scale bar: 25 μm). Comparisons were made using the Student's t-test; ns: no significant difference, $^{**}p < 0.01$, $^{***}p < 0.001$

To detect whether Man-NPs were preferentially absorbed by K7 cells and TAM2, we first polarized BMDMs into TAM1 or TAM2, and then incubated them with coumarin-6-loaded Man-NPs and NPs for 6 h. The mean fluorescence intensity of the Man-NPs absorbed by the K7 cells and TAM2 in the flow cytometry assay was higher than that of the unmodified NPs. The cellular uptake efficiency of the Man-NPs was significantly lower when the cells were pre-treated with free mannose. Additionally, due to the low expression of CD206, TAM1 almost equally absorbed Man-NPs and NPs (Fig. 1e–g; Additional file 1: Fig. S2d). The CLSM assay results were consistent

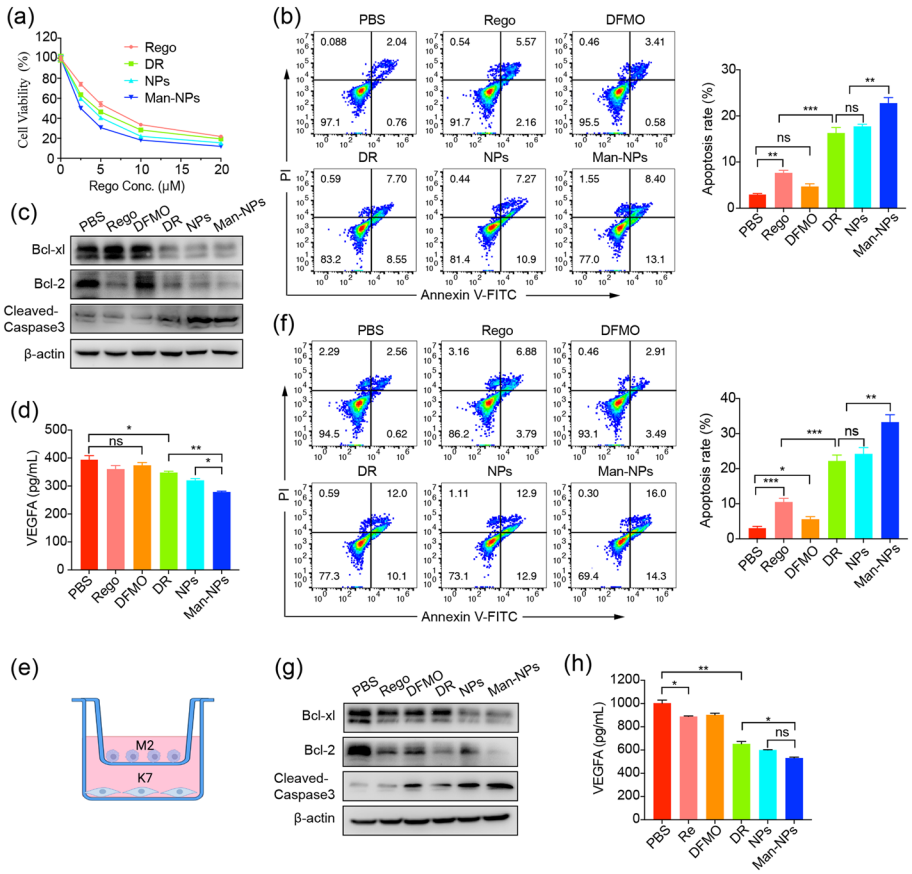

Fig. 2 In vitro anti-tumor effect of Man-NPs. **a** Cytotoxicity study for K7 cells treated with drugs for 48 h. **b** Apoptosis assay of K7 cells via FACS. The right panel displayed the results of the apoptosis rate. **c** Western blotting was used to detect apoptotic protein. **d** VEGFA level of K7 cells after treatment. **e** Schematic of the transwell co-culture model. **f** FACS assay for measuring apoptosis in K7 cells co-cultured with TAM2. The right panel displayed the results of the apoptosis rate. **g** Western blotting was used to identify the apoptotic protein produced by K7 cells co-cultured with TAM2. **h** VEGFA levels in K7 cells co-cultured with TAM2. Comparisons were made using one-way ANOVA with Tukey's test; ns: no significant difference, $^{*}p < 0.05$, $^{**}p < 0.01$, $^{***}p < 0.001$

with flow cytometry (Fig. 1h, i), confirming the theory that Man-NPs are more readily taken up by cells when the mannose receptor mediates them. These findings suggested that the mannose receptor is a key target in mediating drug delivery.

In vitro cytotoxicity

The therapeutic effect should be enhanced owing to the increased cellular uptake of Man-NPs by K7 cells. To validate this, we assessed the anticancer activity of Man-NPs by CCK-8 assay. Compared to free regorafenib, DR, or unmodified NPs, Man-NPs significantly inhibited the proliferation of the K7 cells in a dose- and time-dependent manner and had the lowest IC_{50} value (Fig. 2a; Additional file 1: Fig. S3a-b). However, approximately 90% of TAM1 and TAM2 did not experience any side effects and tolerated the Man-NPs and NPs treatment well (Additional file 1: Fig. S3c). Regorafenib inhibits cancer cell growth by inducing apoptosis and deactivating the AKT and ERK signaling pathways (Pan et al. 2019; Weng et al. 2019). Through the suppression of the MAPK/

ERK and AKT/mTOR signaling pathways, DFMO slows the progression of esophageal cancer (Xie et al. 2020). Man-NPs demonstrated strong anti-tumor efficacy in this study by significantly suppressing the expression of p-AKT, p-MAPK, p-ERK, and p-mTOR (Additional file 1: Fig. S3d), known as signaling pathways for cell survival and growth. Furthermore, Man-NPs were used to test K7 cells for cell apoptosis. In comparison to other treatments, Man-NPs caused a higher rate of apoptosis in K7 cells, as shown in Fig. 2b. Additionally, following Man-NPs treatment, the expression of cleaved-caspase3 was increased. The anti-apoptotic proteins Bcl-xl and Bcl-2 were significantly down-regulated (Fig. 2c). One of the crucial cytokines in TME is VEGF. VEGFA, a member of the VEGF family primarily released by cancer cells and TAMs, is essential for tumor angiogenesis (Valkovic et al. 2002). Meanwhile, VEGFA is an immunosuppressive agent that can suppress T cell activity while inducing the accumulation of Tregs (Bourhis et al. 2021). Compared to unmodified NPs, the secretion of VEGFA significantly decreased after Man-NPs treatment (Fig. 2d).

We used a transwell co-culture model to examine how TAMs affect tumor cells while accurately simulating the physiological conditions of all cells exposed to the drug in TME. In the transwell co-culture system of K7 cells and TAM2 (Fig. 2e), Man-NPs also increased the rate of apoptosis (Fig. 2f) and the expression of apoptosis-related proteins (Fig. 2g), which reduced VEGFA secretion compared to other groups (Fig. 2h).

In vitro polarization and repolarization of macrophages

TAMs are highly dynamic and malleable with reversible polarization between M1 and M2 phenotypes, and they have a variety of roles that include involvement in tumor growth, metastasis, angiogenesis, and immunosuppression (Dallavalasa et al. 2021). Numerous studies have shown that lung metastasis and a poor prognosis in patients with osteosarcoma were significantly correlated with a high density of TAM2 infiltration (Song et al. 2020; Yang et al. 2021). Therefore, reprogramming TAMs is a potential method for treating osteosarcoma without immunosuppression. Figure 3a showed a schematic representation of how BMDMs are converted into macrophages with the M1 and M2 phenotypes. The phenotypes of the macrophages were analyzed by western blot. Man-NPs treatment significantly reduced CD206 expression, suggesting that Man-NPs were successful in reversing TAM2 polarization (Fig. 3b). Man-NPs reversed the polarization toward TAM2 in the transwell co-culture system of TAMs and K7 cells (Fig. 3c), as demonstrated by the downregulation of CD206 (Fig. 3d). The mRNA expression of macrophage biomarkers, including CD86, TNF-α, CD206, and TGF-β, were detected using qRT-PCR to validate this finding further. As shown in Fig. 3e, f, Man-NPs significantly reduced the expression of CD206 and TGF-β (M2 markers) in both TAM1 and TAM2 while substantially increasing the expression of CD86 and TNF-α (M1 marker) in comparison to the untreated cells. IL-10 produced by TAMs can reduce the anti-tumor effect by inhibiting the antigen-presenting cells and reducing T cell effector capabilities like cytotoxicity (Ouyang et al. 2019). The Man-NPs treatment significantly decreased the levels of pro-tumor cytokine IL-10 (Fig. 3g), a stimulator of STAT3 (Verma et al. 2012). Inhibiting the STAT3 signaling pathway can cause macrophage phenotype to change from M2 to M1, as phosphorylated STAT3 is an essential step in

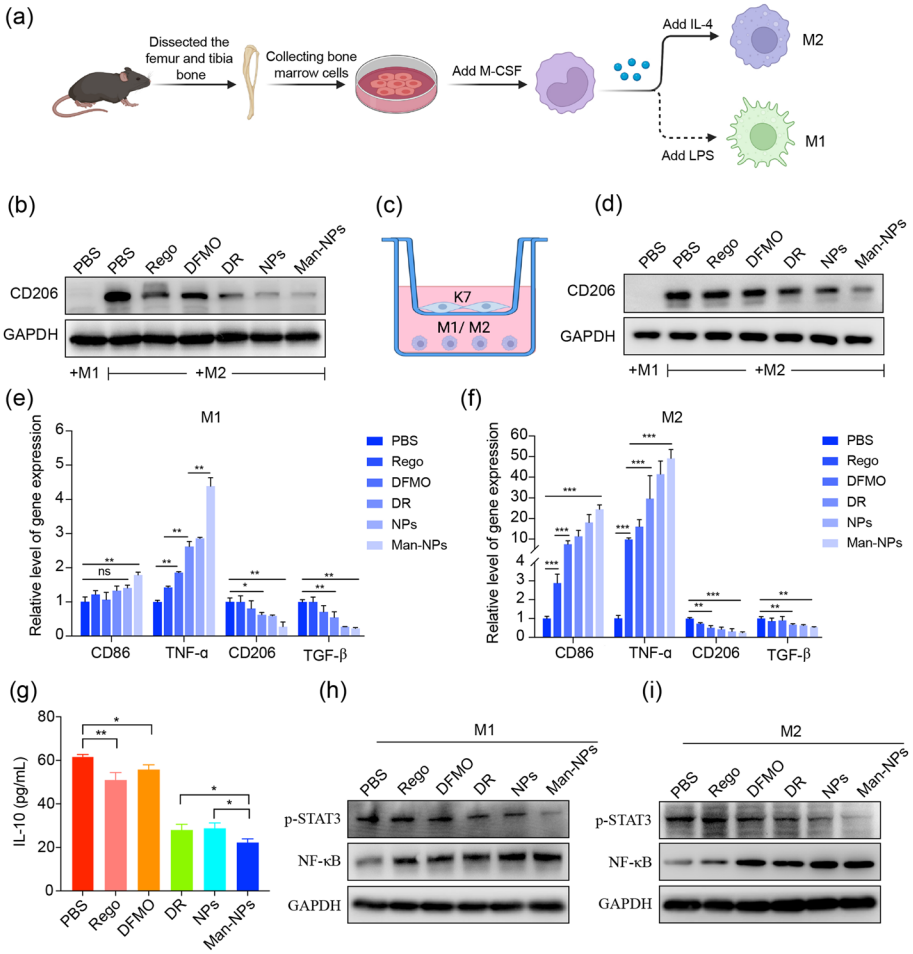

Fig. 3 In vitro control of macrophage repolarization. **a** Schematic illustration of BMDMs isolation, culture, and stimulation. **b** CD206 expression were detected by western blotting in TAMs after drug treatment. **c** Schematic of the transwell co-culture model. **d** The expression of CD206 in the drug-treated TAM2 co-cultured with K7 cells. The mRNA levels of CD86, TNF-α, CD206, and TGF-β in the drug-treated TAM1 (**e**) and TAM2 (**f**) co-cultured with K7 cells. **g** ELISA analysis of the amount of secreted IL-10 in the co-culture of K7 cells and TAM2 after drug treatment. Expression of p-STAT3 and NF-κB in TAM1 (**h**) and TAM2 (**i**) co-cultured with K7 cells after drug treatment. Comparisons were made using one-way ANOVA with Tukey's test; ns: no significant difference, $^{*}p < 0.05$, $^{**}p < 0.01$, $^{***}p < 0.001$

TAM2 polarization (Solis-Martinez et al. 2018). Our findings showed that Man-NPs inhibited STAT3 phosphorylation in TAM1 and TAM2, which was in accordance with a prior study of the effect of DFMO on macrophage polarization through the STAT3 pathway (Alexander et al. 2020). Man-NPs in the TAMs/K7 transwell co-culture system increased pro-inflammatory NF-κB, essential for immune and inflammatory responses, through STAT3 inhibition (Fig. 3h, i). Together, our data suggested that Man-NPs strongly encourage TAM2 repolarization and have the potential to remodel TIME.

In vitro anti-angiogenesis by Man-NPs

An important proof called tumor angiogenesis is what gives rapidly expanding malignant tumors their essential nutrients and oxygen. Several studies have demonstrated that TAMs, particularly TAM2, are crucial for developing abnormal blood vessels in

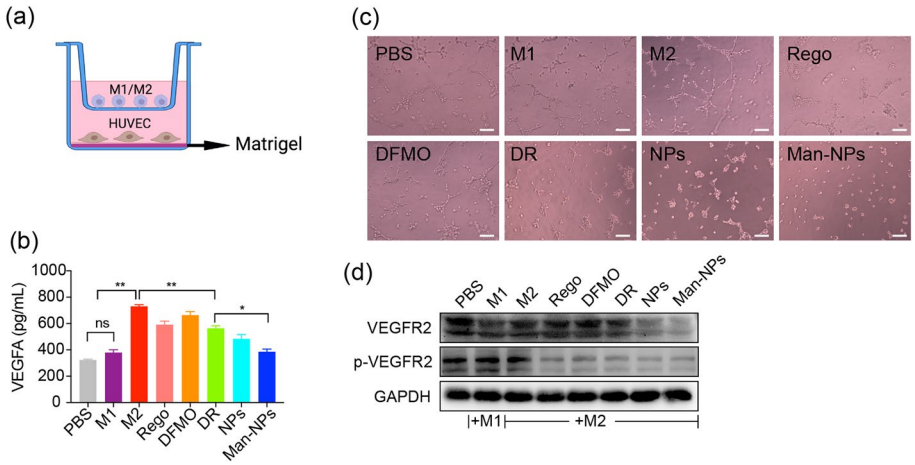

Fig. 4 Anti-angiogenic effect of Man-NPs. **a** Schematic of a transwell co-culture model. **b** The level of VEGFA in the drug-treated TAM1 or TAM2 co-cultured with HUVEC. **c** Tube formation assay in the drug-treated TAM1 or TAM2 co-cultured with HUVEC (scale bar: 100 μm). **d** Expression of VEGFR2 and p-VEGFR2 in HUVEC was detected by Western blotting. Comparisons were made using one-way ANOVA with Tukey's test; ns: no significant difference, $*p < 0.05$, $**p < 0.01$

tumors because they increase VEGF release (Riabov et al. 2014). During the development of tumors, VEGF interacts with the VEGF receptor (VEGFR) on endothelial cells to promote endothelial cell proliferation and migration and angiogenesis close to the tumor site (Dallavalasa et al. 2021). Thus, in the transwell co-culture system of TAMs and HUVEC (Fig. 4a), anti-angiogenesis was investigated using the Matrigel tube formation assay. According to Fig. 4b, TAM2 was primarily responsible for producing VEGF secretion, which was significantly decreased in co-cultured TAM2 cells with HUVEC after Man-NPs treatment. In the capillary-like network, TAM1 inhibited tube formation while TAM2 encouraged it. Man-NPs blocked this encouraged effect as a result of TAM2 repolarization toward TAM1 (Fig. 4c). Furthermore, Man-NPs inhibited the expression of VEGFR2 and p-VEGFR2 in HUVEC (Fig. 4d), which demonstrated a potent anti-angiogenesis effect. These results revealed that Man-NPs inhibit VEGFA/VEGFR2 signaling and regulate macrophage polarization to inhibit tumor angiogenesis.

In vivo tissue biodistribution

The tissue biodistribution of IR780-labeled nanoparticles were investigated in the K7 osteosarcoma tumor-bearing model to evaluate the in vivo tumor-targeting capability of Man-NPs. As shown in Fig. 5a–e, the IR780-labeled NPs and the Man-NPs were successfully delivered to the tumor site. Still, at all times studied, the Man-NPs-treated mice displayed a superior tumor accumulation to the unmodified NPs-treated mice. Ex vivo fluorescent images of the excised tumors further demonstrated that Man-NPs-treated groups had higher tumor accumulation than NPs-treated groups, suggesting that the targeting function provided by the mannose receptor is beneficial.

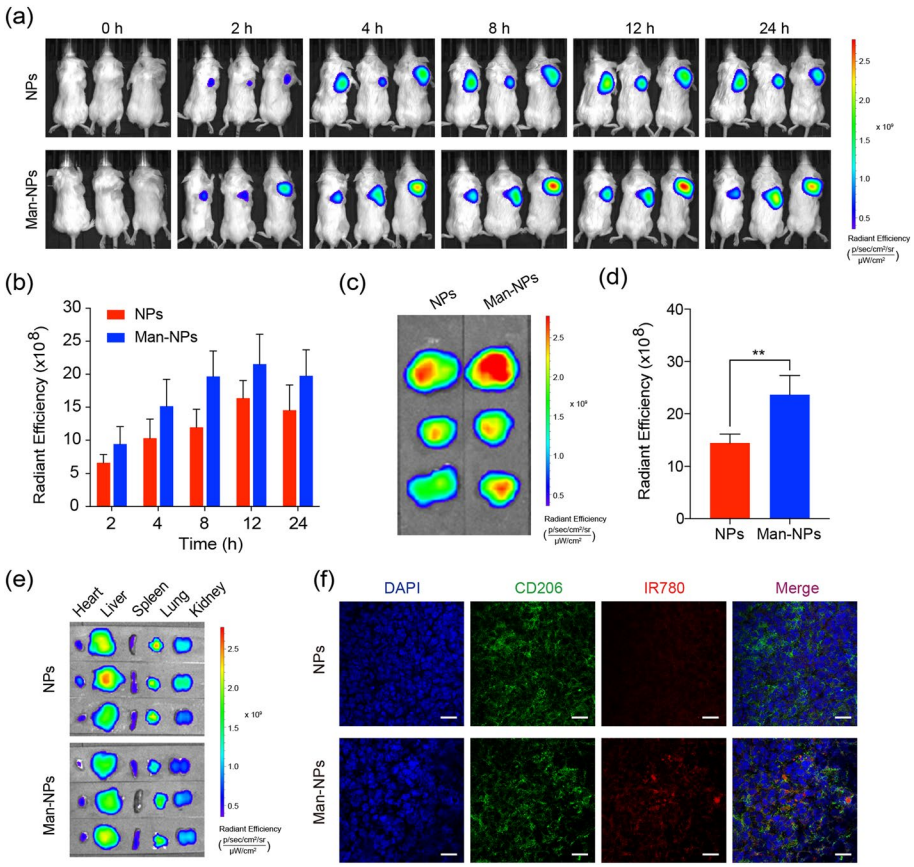

Fig. 5 In vivo imaging and drug-targeting delivery of Man-NPs. **a** Fluorescence imaging was used to detect drug accumulation in the tumors. **b** Radiant efficiency in vivo at the tumor sites. **c** Ex vivo fluorescence imaging of tumors. **d** Ex vivo radiant efficiency of tumors. **e** Ex vivo fluorescence imaging of major organs. **f** The intratumoral distribution of the IR780-loaded Man-NPs with staining of CD206 (scale bar: 25 μm). Comparisons were made using the Student's t-test; $^{**}p < 0.01$

Furthermore, the colocalization of CD206 and Man-NPs was performed to measure intratumoral penetration using immunofluorescent staining. The intratumoral distribution of IR780-labeled Man-NPs was largely consistent with the expression of CD206, as demonstrated by the immunofluorescence imaging (Fig. 5f). According to all of the findings above, the ability of Man-NPs to target tumors is due to the relatively higher phagocytosis of TAMs and cancer cells based on the mannose receptor.

In vivo anti-tumor efficacy and safety evaluation

The murine K7 osteosarcoma subcutaneous tumor model was used to calculate the impact of Man-NPs on tumor growth inhibition in vivo. Anti-tumor therapy was started on the eighth day following subcutaneous injection, and the drugs were injected intravenously every other day for approximately two weeks, as shown in Fig. 6a. The rates of tumor growth inhibition in the Regorafenib and DFMO groups were 39.0% and 22.7%, respectively, while the DR group increased the rate to 56.8%. The strongest anti-tumor effect was seen in Man-NPs group, with a tumor inhibition rate of 69.8% compared to 59.9% in the NPs group. Furthermore, the Man-NPs

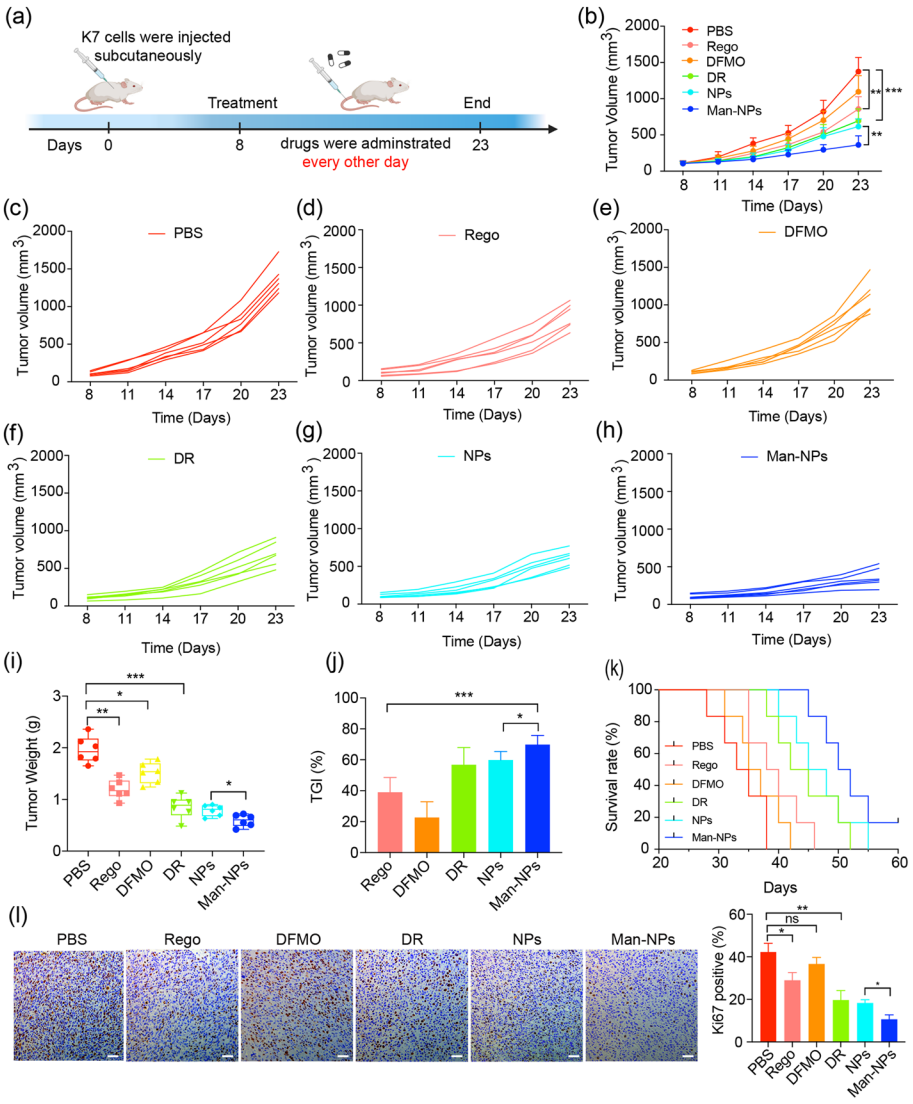

Fig. 6 In vivo therapeutic efficacy of Man-NPs. **a** A schematic illustration of the treatment schedule. **b** The tumor growth curve in K7 subcutaneous tumor-bearing mice following drug treatment (n = 6). (**c**–**h**) Individual tumor growth curves in different groups (n = 6). Tumor weight (**i**), tumor growth inhibition ratio (**j**) and survival curve (**k**) after drug treatment (n = 6). **l** Immunohistochemical staining (brown color) of Ki-67 (scale bar: 50 μm). The right panel displayed the percentage of Ki67 positive results. Comparisons were made using one-way ANOVA with Tukey's test; ns: no significant difference, *$p < 0.05$, **$p < 0.01$, ***$p < 0.001$

group in tumor-bearing mice had the longest survival time (Fig. 6b–k). The lowest cell proliferation capacity was observed by Ki67 staining assays following Man-NPs treatment, which was consistent with tumor growth inhibition (Fig. 6l). Our findings demonstrated the value of targeted delivery for enhancing anti-cancer effectiveness.

Additionally, the preliminary biosafety of Man-NPs was evaluated. The main organs (heart, liver, spleen, lung, and kidney) did not significantly change pathologically during treatment, nor was there any obvious loss of body weight (Additional file 1: Fig. S4a, b). These results indicated that Man-NPs are nontoxic to these organs and exhibit strong biosafety.

In vivo remodeling TIME and inhibiting angiogenesis

The in vivo repolarization of TAMs was assessed by measuring the proportion of M1/M2 phenotype, cytokine secretion, and the expression profile of biomarker proteins to investigate the promising immunotherapeutic effects of Man-NPs. A flow cytometry assay detected the proportion of TAMs of various phenotypes within the tumor tissues. Intratumor TAMs in the PBS group primarily comprised of M2 phenotype ($F4/80^+CD206^+$) while M1 phenotype macrophages ($F4/80^+CD86^+$) were rarely expressed, which may have contributed to the rapid tumor growth. Regorafenib and DFMO, either alone or in

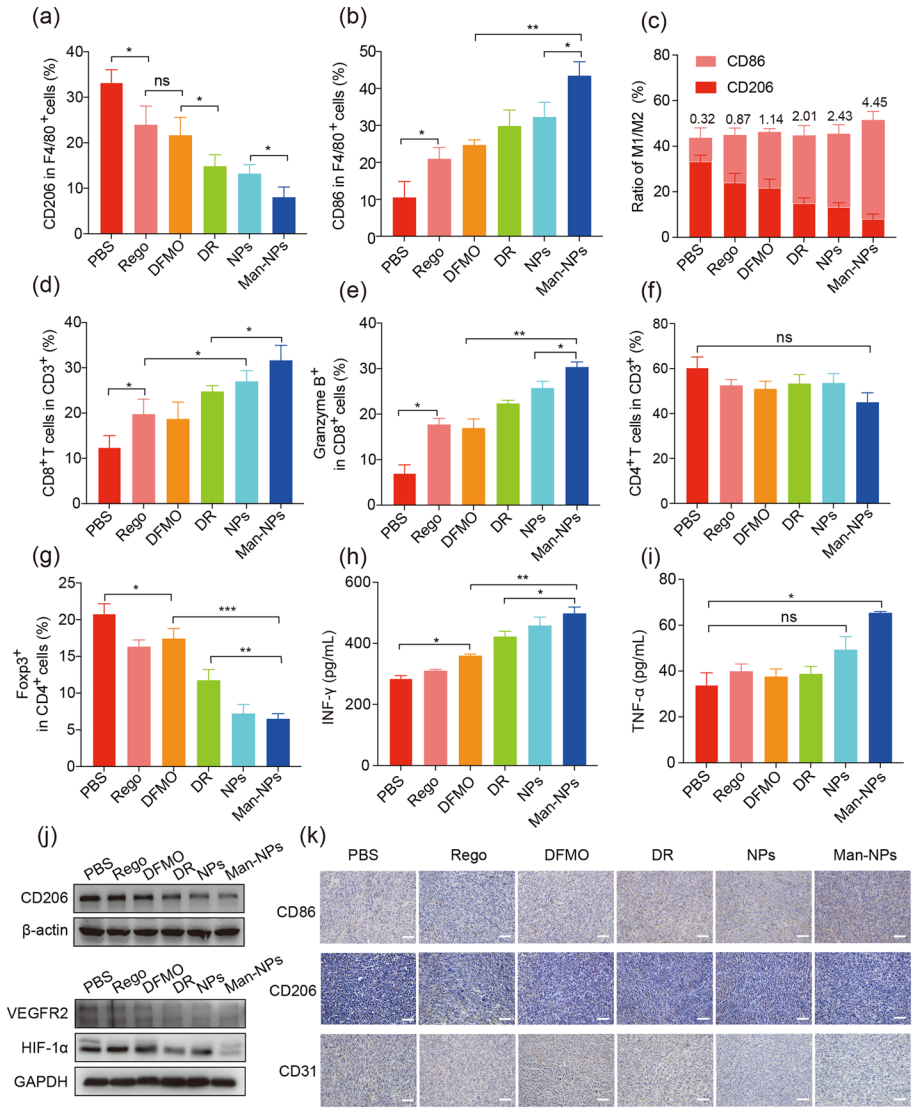

Fig. 7 In vivo remodeling TME. The percentage of TAMs with $CD206^+$ (**a**) and $CD86^+$ cells (**b**) was determined by FACS in subcutaneous tumor tissues. **c** The intratumoral ratio of $CD86^+$ M1/CD206 + M2 phenotype. The percentage of $CD8^+$ cells (**d**) and granzyme B^+ $CD8^+$ T cells (**e**) in intratumoral infiltration. The percentage of $CD4^+$ cells (**f**) and $Foxp3^+$ $CD4^+$ T cells (**g**) in intratumoral infiltration. ELISA analysis of intratumoral cytokine secretion of IFN-γ (**h**) and TNF-α (**i**). **j** The expression of CD206, HIF-1α and VEGFR2 were detected by western blotting in subcutaneous tumor tissues after drug treatment. **k** Immunohistochemical staining (brown color) of CD86, CD86, and CD31 (scale bars: 100 μm). Comparisons were made using one-way ANOVA with Tukey's test; ns: no significant difference, $^*p < 0.05$, $^{**}p < 0.01$, $^{***}p < 0.001$

combination, increased the proportion of M1 phenotype macrophages and decreased the proportion of M2 phenotype macrophages. At the same time, the Man-NPs treatment group showed more noticeable changes (Fig. 7a, b; Additional file 1: Fig. S5a, b). The proportion of M1/M2, which is related to the polarization effect (Zhao et al. 2021), was analyzed to more accurately estimate the in vivo polarization capacity of Man-NPs. As shown in Fig. 7c, the population of total TAMs remained fairly constant among the various groups. Still, the ratio of M1($CD86^+$)/M2 ($CD206^+$) of the Man-NPs group was remarkably higher than that of other treatment groups, suggesting that Man-NPs targeted delivery of nanomedicine may have effectively in vivo reprogrammed macrophages from M2 to M1 phenotype.

It is known that TAM2 can suppress the immune system by preventing tumor-infiltrating lymphocytes from activating (Kuroda et al. 2021). We also conducted a quantitative analysis of $CD4^+$ helper T cells and $CD8^+$ cytotoxic T cells to evaluate the activation of the anti-tumor immune reaction following various treatments. As shown in Fig. 7d–g and Additional file 1: Fig. S5c, d, the Man-NPs treatment significantly increased the tumor population of cytotoxic $CD8^+$ granzyme B^+ T lymphocytes to 29.4%, compared to 6.9% in the PBS group. In contrast, the population of $CD4^+$ T cells barely changed among the various groups. Notably, compared to the other groups, there was a significantly lower percentage of intratumor infiltrating $CD4^+$ $Foxp3^+$ T cells (Tregs), which are associated with immune evasion and a poor prognosis in patients with cancer (Dannenmann et al. 2013). Additionally, following Man-NPs treatment, elevated $CD8^+$ T lymphocytes and declined $CD4^+$ T cells in the spleen were detected (Additional file 1: Fig. S5e). TAM1 and $CD8^+$ T cells produce immunogenic cytokines like IFN-γ and TNF-α to improve the immune response against tumors (Le et al. 2021). Therefore, ELISA was used to determine the intratumoral cytokine levels. The levels of anti-tumor IFN-γ and TNF-α were increased after treatment with Man-NPs due to the enhancement of TAM1 and $CD8^+$ T cells in the tumor tissues (Fig. 7h, i). These findings showed that macrophage repolarization increased immune response activation, which helped to remodel the TIME.

In addition to analyzing the ratio of M1/M2 macrophages and cytokine secretion, western blotting and immunohistochemical staining were used to determine the expression profiles of macrophage surface proteins (CD206 for M2 marker and CD86 for M1 marker) and angiogenic marker proteins (VEGFR2, HIF-1α, and CD31) to further confirm the polarization ability and anti-angiogenesis of Man-NPs. As shown in Fig. 7j, k, the results of the proportion of M1/M2 macrophages were consistent with the intratumoral CD206 expression, which was downregulated, while CD86 expression was upregulated after Man-NPs treatment. The expression of the angiogenic proteins HIF-1α and VEGFR2 was downregulated, which impacted the tumor vessel density (CD31 staining). According to all the findings above, Man-NPs could reprogram TME by boosting TAMs polarization, immune cell infiltration, and angiogenesis inhibition to improve anti-tumor activity in vivo.

Conclusions

In this study, we designed a combination therapy for osteosarcoma that targets TME by dual modulation on TAMs and angiogenesis using a mannosylated PLGA-PEG biomimetic system containing regorafenib and DFMO. By encouraging macrophage polarization from the pro-tumorigenic M2 to the anti-tumorigenic M1 phenotype and inhibiting angiogenesis, the prepared Man-NPs could produce a synergic anti-tumor efficacy with negligible systemic toxicity. Additionally, macrophage repolarization increased immune effector cell activation (e.g., increased $CD8^+$ T cell infiltration and decreased Tregs), which helped to remodel the osteosarcoma TME. These excellent results demonstrated the effectiveness of Man-NPs as a targeted, safe, and powerful anti-tumor nanomedicine, suggesting that it may be a promising immunotherapeutic approach for treating osteosarcoma, with strong development and translational potential.

Materials and methods

Materials

Regorafenib, alpha-difluoromethylornithine, and Coumarin-6 were purchased from MedChemExpress (Monmouth Junction, NJ, USA). Shandong Academy of Pharmaceutical Sciences (China) provided $PLGA_{10K}$-PEG_{5K}-NH_2. Poly(vinyl alcohol) [PVA, 87–89% hydrolyzed, molecular weight (Mw) 31,000–50,000], lipopolysaccharide (LPS), 1-ethyl-3-(3-dimethylaminopropyl)-carbodiimide hydrochloride (EDC), and IR 780 iodide were purchased from Sigma Aldrich (St. Louis, MO, USA). Bide Pharmatech Ltd. (Shanghai, China) provided the A-D-mannosylphenyl isothiocyanate. We purchased sulfo-N-hydroxysuccinimide (NHS) from Aladdin Holdings Group Co., Ltd. (Beijing, China). Murine IL-4 and M-CSF were supplied by PeproTech (Rocky Hill, NJ, USA).

Mannose receptor (CD206), CD31, and β-Actin were received from Abcam (UK). Bcl-2, Bcl-xl, cleaved-caspase3, p-STAT3, NF-κB, VEGFR2, p-VEGFR2, p-MAPK, p-ERK, p-mTOR, Ki-67, and GAPDH were provided with Cell Signaling Technology (USA). R&D Systems (USA) provided fixable viability stain 620 and APC-Cy7 anti-mouse CD45. The following antibodies were obtained from BioLegend (USA): FITC anti-mouse/human CD11b, PerCP-Cy5.5 anti-mouse F4/80, Pacific Blue™ anti-mouse CD86, PE/Cy7 anti-mouse CD206, FITC anti-mouse CD45, APC- Fire™ 750 anti-mouse CD3, PE-Cy7 anti-mouse CD4, PerCP-Cy5.5 anti-mouse CD8 alpha, PE anti-mouse CD25, Alexa Fluor® 647 anti-mouse Foxp3, and AF700 anti-mouse Granzyme B. MultiSciences Biotech Co., Ltd (Hangzhou, China) provided an enzyme-linked immunosorbent assay (ELISA) kit for the detection of mouse VEGFA, IL-10, tumor necrosis factor-alpha (TNF-α), and interferon-gamma (IFN-γ). Sinapharm Chemical Reagent Co., Ltd. (Shanghai, China) provided all other substances.

Synthesis of the drug-encapsulated nanoparticles

A prior study used a double emulsion solvent evaporation method to create the drug-encapsulated NPs (Zambito et al. 2021). Briefly, 3 ml of dichloromethane (DCM) containing 300 mg PLGA-PEG (organic phase) were combined with 5 mg DFMO solution

(100 μL deionized water) as the first aqueous phase. Then, while stirring, 100 μL of DMSO containing 1 mg of regorafenib was added to the polymer-DCM solution. Using ultrasound on ice for 30 s, the primary water in oil (w/o) emulsion was obtained. The primary emulsion was then added to 15 mL of 1.0% (w/v) PVA water solution and homogenized using an ultrasonic device in an ice bath for 30 min. The water–oil-water (w/o/w) emulsion was then added to 50 mL of 0.3% PVA and stirred slowly overnight at room temperature (RT) to sanction the solvent to evaporate and nanoparticles to solidify. Finally, NPs were lyophilized, stored at − 20 °C until further use, and rinsed with deionized water three times. Similar techniques were used to create NPs loaded with coumarin-6 or IR780.

Preparation and characterization of Man-NPs

A-D-mannosylphenyl isothiocyanate was attached to the surface of drug-encapsulated NPs to create Man-NPs. Briefly, 10 mg of NHS and 10 mg of EDC were added to 100 mg of NPs dissolved in 10 mL MES buffer (pH 5.0) and stirred for 2 h. The mixture solution was given 100 mg of A-D-mannosylphenyl isothiocyanate and was stirred overnight at RT. Following a 12 h period, Man-NPs were precipitated with cold diethyl ether and methanol and dried under a vacuum. The co-polymer was precipitated, washed with cold methanol, and dried under a vacuum to remove unreacted mannose and excess reagents. H^1NMR spectrum of synthesized Man-PLGA-PEG was used to identify its chemical composition in CDCl3.

The dynamic light scattering measurement (Malvern, UK) was used to determine the particle size, zeta potential, and polydispersity index (PDI) of the NPs. The morphology of the NPs was observed using transmission electron microscopy (H-7650; Hitachi, Japan). The encapsulation efficiency and drug-loading capacity of regorafenib in NPs were determined by high-performance liquid chromatography (HPLC) equipped with Agilent-C18 (4.6 × 250 mm, 5 μm) column (1260 Infinity, Agilent Technologies, USA) with a flow rate of 0.5 mL/min and column temperature of 35 °C. The mobile phase contained 0.5% KH2PO4 (pH 3.5) and 70% acetonitrile, and the detection wavelength was 260 nm. By using liquid chromatography-mass spectrometry (LCMS) and an Acquity UPLC BEH C18 (2.1 × 100 mm, 1.7 μm) column (ACQUITY QDa, Waters Corp., USA) with a flow rate of 0.3 mL/min and column temperature of 35 °C, the encapsulation efficiency and drug-loading capacity of DFMO in NPs were detected. 100% acetonitrile and 0.1% formic acid aqueous solution made up the mobile phase. The calculation was as follows:

$$\text{Encapsulation efficiency (\%)} = \left(\text{mass of encapsulated drug}\right)/\left(\text{mass of drug added}\right) \times 100\%$$

$$\text{Drug-loading capacity (\%)} = \left(\text{mass of encapsulated drug}\right)/\left(\text{mass of NPs}\right) \times 100\%$$

Stability of NPs and in vitro drug release

The NPs were dissolved in phosphate buffer saline (PBS) containing 10% FBS to assess the stability. At various time points, the NPs changing particle size was examined. Cumulative in vitro drug release of Man-NPs was evaluated using a dialysis method.

Man-NPs were placed into a dialysis bag (MWCO, 8–14 kDa), suspended in a mixed solution of PBS with 0.05% SDS and 60% methanol at two different pH values (7.4 and 6.5), and then gently shaken at 100 rpm at 37 °C. A corresponding amount of fresh medium was added, and 1 mL of the release medium was taken at the specified time to measure the concentration of regorafenib by HPLC.

Cell culture

American Type Culture Collection (Manassas, VA, USA) provided the murine osteosarcoma cell line K7, RAW264.7 and human umbilical vein endothelial cells (HUVEC). K7 cells and RAW264.7 were cultured in DMEM containing 10% FBS plus 1% penicillin/streptomycin (Gibco, USA). HUVEC were cultured in the endothelial cell medium (ECM) supplemented with 5% FBS, and 1% endothelial cell growth supplement (ECGS) (ScienCell, USA). All cell lines were maintained in a 37 °C incubator with 5% carbon dioxide and 95% air.

Collection and polarization of bone marrow-derived macrophages (BMDMs)

As previously described (Pineda-Torra et al. 2015), C57BL/6 mice's femurs and tibias were used to collect bone marrow cells. The cells were cultured in RPMI 1640 medium with 10% FBS and 20 ng/mL M-CSF for 5 days to promote differentiation into BMDMs. Following differentiation, BMDMs were stimulated for 24 h with either 100 ng/mL LPS or 40 ng/mL IL-4 to polarize them into the M1 or M2 phenotypes, respectively. The macrophage phenotypic marker was further detected using real-time quantitative polymerase chain reaction (qRT-PCR), western blotting, and ELISA.

In vitro cellular uptake study

The K7 cells were cultured in a 6-well plate and 35-mm confocal dishes for 24 h with 2×10^5 cells/well or 1×10^5 cells/dish. The coumarin-6-loaded NPs and Man-NPs were added to the cells and incubated for 6 h. Coumarin-6 was quantified by fluorescence spectrophotometer (Hitachi, Japan) with an excitation wavelength of 420 nm and an emission wavelength of 506 nm. The cells were pre-treated with mannose (100 mM) for 4 h in a parallel group before incubating with the Man-NPs (Su et al. 2015). The cellular uptake efficiency was then measured using a flow cytometer assay (BD Biosciences, USA). Additionally, the cells in confocal dishes underwent three PBS washes, a 15 min fixation in 4% paraformaldehyde and DAPI staining, and were observed under a confocal laser scanning microscope (CLSM; TCS-SP8, Leica, Germany). Similarly, the cellular uptake of stimulated macrophages was carried out as described above.

In vitro cytotoxicity study

The K7 cells were plated in the 96-well plates at a density of 4000 cells per well and cultured for 24 h. Free regorafenib, DFMO, combined DFMO and regorafenib (DR), NPs, or Man-NPs, were all used to treat the cells. According to the manufacturer's instructions, cell counting kit-8 (CCK-8; Dojindo) were used to test the viability of the cells after 24 h, 48 h and 72 h of incubation.

Preparation of transwell co-culture model

A transwell system with a 0.4 μm pore membrane (Corning, USA) was used to create a co-culture model. Its purpose was to faithfully reproduce the physiological conditions of TME, where the cells were exposed to the drugs. The transwell system's upper and lower compartments were seeded with TAM1 or TAM2 and K7 cells and co-incubated for 12 h. All cells were exposed to free regorafenib (2 μM), DFMO (1 mM), DR, NPs, or Man-NPs for 24 h. The K7 cells were harvested for further experiments. However, If TAM1 or TAM2 were to be used for analysis, K7 cells would be seeded in the upper compartment to facilitate the collection process.

Similarly, TAM1 or TAM2 was seeded into the transwell system's upper compartment, while HUVECs (2×10^4) cells were cultured in the lower compartment after being treated with a matrigel matrix. Following the above-mentioned treatments, the cells were incubated at 37 °C for 12 h. The capillary network was photographed using the fluorescence microscope (Leica, Germany).

Flow cytometry analysis

The cells were collected after being co-incubated for 24 h, washed, and further stained by an Annexin V-FITC/PI apoptosis detection kit (Thermo Fisher, Waltham, USA) according to the manufacturer's instructions to quantitatively analyze the K7 cell apoptosis rate after drug treatment with or without co-culture. Furthermore, flow cytometry was used to quantitatively analyze the proportion of TAMs and T cells infiltrating tumor and spleen to assess the in vivo polarization ability of Man-NPs. Red blood cells were then separated from the fresh tumor and spleens tissues using red blood cell lysis buffer after the tissues had been cut into slices and digested with hyaluronidase, type IV collagenase, and DNA enzyme. The cells were extracted using lymphocyte separation solution for T cell sorting. Then they were incubated with specific immune cell biomarkers like CD86, CD206, Foxp3, and Granzyme B. After being filtered, the cell suspensions were examined with the FACS Calibur.

Western blot

After treatment, the cells and tumor tissues were harvested and lysed for 30 min in an ice bath using RIPA buffer mixed with a protease and phosphatase inhibitor (Sigma Aldrich, USA). The supernatants were collected after centrifugation at 12,000*g* at 4 °C for 20 min, and the results were determined using the BCA assay (Beyotime, China). The protein samples were separated by SDA-PAGE and then transferred to PVDF membranes (Millipore, USA). After incubating TBST containing 5% non-fat milk for 1 h at RT, these membranes were incubated overnight at 4 °C with primary antibodies. Following a standard procedure, secondary antibodies conjugated to horseradish peroxidase were incubated with the protein bands. Finally, signals were visualized using ECL detection reagents, and the loading control was either GAPDH or β-actin.

qRT-PCR and ELISA

The total RNA was extracted from the macrophages with TRIzol Reagent (Thermo, USA) and was reverse-transcribed into cDNA using the TaKaRa PrimeScript RT Reagent kit (TaKaRa, Japan) according to the manufacturer's instructions. qRT-PCR was

then performed using SYBR® Premix DimerEraser™ (TaKaRa, Japan) following the manufacturer's instructions. mRNA levels were normalized using β-actin as a control. The gene-specific primer sequences are listed in Additional file 1: Table S1. Using ELISA kits following the manufacturer's instructions, the levels of cytokines (VEGFA, IL-10, IFN-γ, and TNF-α) in the culture medium or tumor tissues were determined.

In vivo imaging and biodistribution study

Through the subcutaneous injection of K7 cells (1×10^6 cells) into the back of BALB/c mice (female, 5–6 weeks old), the xenograft osteosarcoma tumor model was created. The mice were randomly divided into two groups when the tumors reached a median size of 500 mm^3. Each mouse received an equal dose of IR780-loaded NPs or Man-NPs injected into the tail vein. Using an IVIS imaging system (Xenogen), the biodistribution of the NPs in mice was studied at various time points. The mice were euthanized after 24 h, and the tumors and major organs were surgically removed for ex vivo imaging. The tissue from the K7 osteosarcoma tumor model was also obtained for cryosection to conduct the co-localization study. Slices were stained with Alexa Fluor 488-conjugated goat secondary antibody for 1 h at RT, followed by DAPI staining. The slices were first incubated with an anti-CD206 antibody at 4 °C overnight. The co-localization was observed using CLSM.

In vivo anti-tumor efficacy and safety evaluation

As mentioned above, the osteosarcoma tumor model was developed in BALB/c mice. For the administration of drugs, the tumor-bearing mice were randomly split into six groups (six mice per group) when the tumor size reached approximately 100 mm^3. PBS (control), regorafenib, DFMO, DR, NPs, and Man-NPs at 5 mg/kg regorafenib and 20 mg/kg DFMO every other day for about two weeks were intravenously injected into each group. Each mouse's tumor volume and body weight were measured to assess anti-tumor efficacy and safety in vivo. The formula used to determine tumor volumes was $V\ (mm^3) = (\text{length} \times \text{width}^2)/2$. For ethical reasons, the mice were euthanized when the biggest tumor approached 2000 cm^3. Tumor tissues and major organs were collected for additional testing. The formula used to determine the tumor growth inhibition ratio (TGI %) was $TGI\ (\%) = (1 - W_{treat}/W_{control}) \times 100\%$ ($W_{control}$ and W_{treat} represent the tumor weight of the control and treatment groups, respectively). The Shanghai General Hospital Animal Ethics Committee reviewed and approved all experiments and procedures to ensure they complied with ethical regulations.

Statistical analysis

All data were analyzed using Graphpad Prism 8 and IBM statistical package for social sciences 18. Data were presented as mean ± standard deviation, and each experiment was carried out in triplicate. The student's t-test was applied to compare the differences between the two groups. One-way analysis of variance (ANOVA) was applied when more than two groups were involved. The outcomes of animal survival were compared using the log-rank (Mantel-Cox) test. Statistically significant difference was denoted as $^{*}P < 0.05$, $^{**}P < 0.01$, and $^{***}P < 0.001$.

Abbreviations

TME	Tumor microenvironment
TAMs	Tumor-associated macrophages
PBT	Polyamine blocking therapy
DFMO	Alpha-difluoromethylornithine
VEGF	Endothelial growth factor
VEGFA	Endothelial growth factor receptor
HUVEC	Human umbilical vein endothelial cells
BMDMs	Bone marrow-derived macrophages
PLGA-PEG	Poly(lactide-co-glycolide)-polyethylene glycol
LPS	Lipopolysaccharide
NHS	Sulfo-N-hydroxysuccinimide
EDC	1-Ethyl-3-(3-dimethylaminopropyl)-carbodiimide hydrochloride
TEM	Transmission electron microscopy
HPLC	High-performance liquid chromatography
LCMS	Liquid chromatography-mass spectrometry
CLSM	Confocal laser scanning microscope

Supplementary Information

The online version contains supplementary material available at https://doi.org/10.1186/s12645-023-00186-7.

Additional file 1: Fig. S1 H1NMR detection of Man-PLGA-PEG. Fig. S2Zeta potential of the NPs and Man-NPs.Stability of Man-NPs in PBS containing 10% FBS.Uptake of NPs and Man-NPs with or without pretreatment with mannose in K7, TAM2, and TAM1. Fig. S3Cytotoxicity study for K7 cells treated with drugs for 24 h and 72 h.IC50 values of the free regorafenib, DR, NPs, and Man-NPs in the K7 cells.Cytotoxicity of NPs and Man-NPs to BMDMs.The expression of p-AKT, p-MAPK, p-ERK and p-mTOR in K7 cells were detected by western blotting following drug treatment. Fig. S4 Preliminary safety evaluation.The body weight changes of K7 subcutaneous tumor-bearing mice after drug treatment.Images of H&E staining of several major organ sections after drug treatments. Fig. S5 Identification of immune cell phenotype and subpopulation in the tumor and spleen tissues were detected by FACS in K7 subcutaneous tumor model. The proportion of CD206+, and CD86+ macrophagesin the tumor tissues.The proportion of granzyme B+ CD8+ T cells.The proportion of Foxp3+ CD4+ T cells.The percentage of CD4+ cells and CD8+ in CD3+ cells in the spleens tissues. Table S1.Gene primers used for qRT-PCR.

Acknowledgements

We are particularly grateful to Nanjing Nanoeast Biotech Co., Ltd for providing technical support in the synthesis of the drug-encapsulated nanoparticles. HPLC and H1NMR spectrum was performed by Dr Ling Huang at Nanjing Nanoeast Biotech Co., Ltd.

Author contributions

WS, XJM, and HSW designed the research; XMJ, YHG, XH, YMX, YFJ, and CY performed experiments and data analysis; XMJ, YHG, HRM, and CY participated in manuscript preparation; ZYW and TZ contributed to the methodology and investigation; YQH and ZDC were involved in project administration and supervision. HSW, JX, XJM, and WS were involved in funding acquisition, resources, writing—review and editing. All authors have read and approved the final manuscript.

Funding

This work was supported by Shanghai Jiaotong University (ZH2018QNA15), the National Natural Science Foundation of China (81902734, 81772859, 82072969, 81972517), Shanghai Pujiang Program (2019PJD043), Shanghai Rising-Star Program (20QA1408000), Songjiang District Science and Technology Innovation Fund (18sjkjgg30).

Availability of data and materials

Data will be made available on request.

Declarations

Ethics approval and consent to participate

All animal experiments have been approved by the Shanghai General Hospital Animal Care and Use Committee (protocol 201601).

Consent for publication

Not applicable.

Competing interests

The authors declare that they have no competing interests regarding this article.

Received: 23 September 2022 Accepted: 1 April 2023
Published online: 09 May 2023

References

Alexander ET, Mariner K, Donnelly J, Phanstiel Ot, Gilmour SK (2020) Polyamine blocking therapy decreases survival of tumor-infiltrating immunosuppressive myeloid cells and enhances the antitumor efficacy of PD-1 blockade. Mol Cancer Ther 19:2012–2022. https://doi.org/10.1158/1535-7163.MCT-19-1116

Bourhis M, Palle J, Galy-Fauroux I, Terme M (2021) Direct and indirect modulation of T cells by VEGF-A counteracted by anti-angiogenic treatment. Front Immunol 12:616837. https://doi.org/10.3389/fimmu.2021.616837

Cersosimo F, Lonardi S, Bernardini G, Telfer B, Mandelli GE, Santucci A et al (2020) Tumor-associated macrophages in osteosarcoma: from mechanisms to therapy. Int J Mol Sci 21:5207. https://doi.org/10.3390/ijms21155207

Chiang IT, Lee YH, Tan ZL, Hsu FT, Tu HF (2022) Regorafenib enhances antitumor immune efficacy of anti-PD-L1 immunotherapy on oral squamous cell carcinoma. Biomed Pharmacother 147:112661. https://doi.org/10.1016/j.biopha.2022.112661

Dallavalasa S, Beeraka NM, Basavaraju CG, Tulimilli SV, Sadhu SP, Rajesh K et al (2021) The Role of tumor associated macrophages (TAMs) in cancer progression, chemoresistance, angiogenesis and metastasis—current status. Curr Med Chem 28:8203–8236. https://doi.org/10.2174/0929867328666210720143721

Dannenmann SR, Thielicke J, Stockli M, Matter C, von Boehmer L, Cecconi V et al (2013) Tumor-associated macrophages subvert T-cell function and correlate with reduced survival in clear cell renal cell carcinoma. Oncoimmunology 2:e23562. https://doi.org/10.4161/onci.23562

Davis LE, Bolejack V, Ryan CW, Ganjoo KN, Loggers ET, Chawla S et al (2019) Randomized double-blind phase II study of regorafenib in patients with metastatic osteosarcoma. J Clin Oncol 37:1424–1431. https://doi.org/10.1200/JCO.18.02374

Doleschel D, Hoff S, Koletnik S, Rix A, Zopf D, Kiessling F et al (2021) Regorafenib enhances anti-PD1 immunotherapy efficacy in murine colorectal cancers and their combination prevents tumor regrowth. J Exp Clin Cancer Res 40:288. https://doi.org/10.1186/s13046-021-02043-0

Duffaud F, Mir O, Boudou-Rouquette P, Piperno-Neumann S, Penel N, Bompas E et al (2019) Efficacy and safety of regorafenib in adult patients with metastatic osteosarcoma: a non-comparative, randomised, double-blind, placebo-controlled, phase 2 study. Lancet Oncol 20:120–133. https://doi.org/10.1016/S1470-2045(18)30742-3

Galon J, Bruni D (2019) Approaches to treat immune hot, altered and cold tumours with combination immunotherapies. Nat Rev Drug Discov 18:197–218. https://doi.org/10.1038/s41573-018-0007-y

Gill J, Gorlick R (2021) Advancing therapy for osteosarcoma. Nat Rev Clin Oncol 18:609–624. https://doi.org/10.1038/s41571-021-00519-8

Hayes CS, Shicora AC, Keough MP, Snook AE, Burns MR, Gilmour SK (2014) Polyamine-blocking therapy reverses immunosuppression in the tumor microenvironment. Cancer Immunol Res 2:274–285. https://doi.org/10.1158/2326-6066.CIR-13-0120-T

Koirala P, Roth ME, Gill J, Piperdi S, Chinai JM, Geller DS et al (2016) Immune infiltration and PD-L1 expression in the tumor microenvironment are prognostic in osteosarcoma. Sci Rep 6:30093. https://doi.org/10.1038/srep30093

Kuroda H, Jamiyan T, Yamaguchi R, Kakumoto A, Abe A, Harada O et al (2021) Tumor microenvironment in triple-negative breast cancer: the correlation of tumor-associated macrophages and tumor-infiltrating lymphocytes. Clin Transl Oncol 23:2513–2525. https://doi.org/10.1007/s12094-021-02652-3

Lacal PM, Graziani G (2018) Therapeutic implication of vascular endothelial growth factor receptor-1 (VEGFR-1) targeting in cancer cells and tumor microenvironment by competitive and non-competitive inhibitors. Pharmacol Res 136:97–107. https://doi.org/10.1016/j.phrs.2018.08.023

Le T, Su S, Shahriyari L (2021) Immune classification of osteosarcoma. Math Biosci Eng 18:1879–1897. https://doi.org/10.3934/mbe.2021098

Lewis EC, Kraveka JM, Ferguson W, Eslin D, Brown VI, Bergendahl G et al (2020) A subset analysis of a phase II trial evaluating the use of DFMO as maintenance therapy for high-risk neuroblastoma. Int J Cancer 147:3152–3159. https://doi.org/10.1002/ijc.33044

Liu Y, Li Q, Bai Q, Jiang W (2021) Advances of smart nano-drug delivery systems in osteosarcoma treatment. J Mater Chem B 9:5439–5450. https://doi.org/10.1039/d1tb00566a

Marchandet L, Lallier M, Charrier C, Baud'huin M, Ory B, Lamoureux F (2021) Mechanisms of resistance to conventional therapies for osteosarcoma. Cancers 13:683. https://doi.org/10.3390/cancers13040683

Okikawa S, Morine Y, Saito Y, Yamada S, Tokuda K, Teraoku H et al (2022) Inhibition of the VEGF signaling pathway attenuates tumorassociated macrophage activity in liver cancer. Oncol Rep 47:71. https://doi.org/10.3892/or.2022.8282

Ou DL, Chen CW, Hsu CL, Chung CH, Feng ZR, Lee BS et al (2021) Regorafenib enhances antitumor immunity via inhibition of p38 kinase/Creb1/Klf4 axis in tumor-associated macrophages. J Immunother Cancer 9:e001657. https://doi.org/10.1136/jitc-2020-001657

Ouyang W, O'Garra A (2019) IL-10 Family cytokines IL-10 and IL-22: from basic science to clinical translation. Immunity 50:871–891. https://doi.org/10.1016/j.immuni.2019.03.020

Pan PJ, Liu YC, Hsu FT (2019) Protein kinase B and extracellular signal-regulated kinase inactivation is associated with regorafenib-induced inhibition of osteosarcoma progression in vitro and in vivo. J Clin Med 8:900. https://doi.org/10.3390/jcm8060900

Pfeffer LM, Yang CH, Pfeffer SR, Murti A, McCormack SA, Johnson LR (2000) Inhibition of ornithine decarboxylase induces STAT3 tyrosine phosphorylation and DNA binding in IEC-6 cells. Am J Physiol Cell Physiol 278:C331-335. https://doi.org/10.1152/ajpcell.2000.278.2.C331

Pineda-Torra I, Gage M, de Juan A, Pello OM (2015) Isolation, culture, and polarization of murine bone marrow-derived and peritoneal macrophages. Methods Mol Biol 1339:101–109. https://doi.org/10.1007/978-1-4939-2929-0_6

Riabov V, Gudima A, Wang N, Mickley A, Orekhov A, Kzhyshkowska J (2014) Role of tumor associated macrophages in tumor angiogenesis and lymphangiogenesis. Front Physiol 5:75. https://doi.org/10.3389/fphys.2014.00075

Samal K, Zhao P, Kendzicky A, Yco LP, McClung H, Gerner E et al (2013) AMXT-1501, a novel polyamine transport inhibitor, synergizes with DFMO in inhibiting neuroblastoma ce ll proliferation by targeting both ornithine decarboxylase and polyamine transport. Int J Cancer 133:1323–1333. https://doi.org/10.1002/ijc.28139

Sholler GLS, Ferguson W, Bergendahl G, Bond JP, Neville K, Eslin D et al (2018) Maintenance DFMO increases survival in high risk neuroblastoma. Sci Rep 8:14445. https://doi.org/10.1038/s41598-018-32659-w
Solis-Martinez R, Cancino-Marentes M, Hernandez-Flores G, Ortiz-Lazareno P, Mandujano-Alvarez G, Cruz-Galvez C et al (2018) Regulation of immunophenotype modulation of monocytes-macrophages from M1 into M2 by prostate cancer cell-culture supernatant via transcription factor STAT3. Immunol Lett 196:140–148. https://doi.org/10.1016/j.imlet.2018.02.009
Song YJ, Xu Y, Zhu X, Fu J, Deng C, Chen H et al (2020) Immune landscape of the tumor microenvironment identifies prognostic gene signature CD4/CD68/CSF1R in osteosarcoma. Front Oncol 10:1198. https://doi.org/10.3389/fonc.2020.01198
Su L, Zhang W, Wu X, Zhang Y, Chen X, Liu G et al (2015) Glycocalyx-mimicking nanoparticles for stimulation and polarization of macrophages via specific interactions. Small 11:4191–4200. https://doi.org/10.1002/smll.201403838
Tawbi HA, Burgess M, Bolejack V, Van Tine BA, Schuetze SM, Hu J et al (2017) Pembrolizumab in advanced soft-tissue sarcoma and bone sarcoma (SARC028): a multicentre, two-cohort, single-arm, open-label, phase 2 trial. Lancet Oncol 18:1493–1501. https://doi.org/10.1016/S1470-2045(17)30624-1
Valkovic T, Dobrila F, Melato M, Sasso F, Rizzardi C, Jonjic N (2002) Correlation between vascular endothelial growth factor, angiogenesis, and tumor-associated macrophages in invasive ductal breast carcinoma. Virchows Arch 440:583–588. https://doi.org/10.1007/s004280100458
Verma SK, Krishnamurthy P, Barefield D, Singh N, Gupta R, Lambers E et al (2012) Interleukin-10 treatment attenuates pressure overload-induced hypertrophic remodeling and improves heart function via signal transducers and activators of transcription 3-dependent inhibition of nuclear factor-kappaB. Circulation 126:418–429. https://doi.org/10.1161/CIRCULATIONAHA.112.112185
Weng MC, Li MH, Chung JG, Liu YC, Wu JY, Hsu FT et al (2019) Apoptosis induction and AKT/NF-kappaB inactivation are associated with regroafenib-inhibited tumor progression in non-small cell lung cancer in vitro and in vivo. Biomed Pharmacother 116:109032. https://doi.org/10.1016/j.biopha.2019.109032
Xie Y, Dong CD, Wu Q, Jiang Y, Yao K, Zhang J et al (2020) Ornithine decarboxylase inhibition downregulates multiple pathways involved in the formation of precancerous lesions of esophageal squamous cell cancer. Mol Carcinog 59:215–226. https://doi.org/10.1002/mc.23144
Yang H, Zhao L, Zhang Y, Li FF (2021) A comprehensive analysis of immune infiltration in the tumor microenvironment of osteosarcoma. Cancer Med 10:5696–5711. https://doi.org/10.1002/cam4.4117
Ye C, Geng Z, Dominguez D, Chen S, Fan J, Qin L et al (2016) Targeting ornithine decarboxylase by alpha-difluoromethylornithine inhibits tumor growth by impairing myeloid-derived suppressor cells. J Immunol 196:915–923. https://doi.org/10.4049/jimmunol.1500729
Zambito G, Deng S, Haeck J, Gaspar N, Himmelreich U, Censi R et al (2021) Fluorinated PLGA-PEG-mannose nanoparticles for tumor-associated macrophage detection by optical imaging and MRI. Front Med 8:712367. https://doi.org/10.3389/fmed.2021.712367
Zhao Y, Zhang B, Zhang Q, Ma X, Feng H (2021) Tumor-associated macrophages in osteosarcoma. J Zhejiang Univ Sci B 22:885–892. https://doi.org/10.1631/jzus.B2100029

Publisher's Note

Springer Nature remains neutral with regard to jurisdictional claims in published maps and institutional affiliations.

Ready to submit your research? Choose BMC and benefit from:

- fast, convenient online submission
- thorough peer review by experienced researchers in your field
- rapid publication on acceptance
- support for research data, including large and complex data types
- gold Open Access which fosters wider collaboration and increased citations
- maximum visibility for your research: over 100M website views per year

At BMC, research is always in progress.

Learn more biomedcentral.com/submissions

BMC